Available online at www.sciencedirect.com
SCIENCE DIRECT®
C. R. Physique 6 (2005) 654–662
COMPTES RENDUS PHYSIQUE
http://france.elsevier.com/direct/COMREN/

Interaction of electromagnetic fields with the environment/Interaction du champ électromagnétique avec l'environnement

# Computation of electromagnetic scattering by multilayer dielectric objects using Gaussian beam based techniques

Alexandre Chabory [a,b], Jérôme Sokoloff [b,*], Sylvain Bolioli [a], Paul François Combes [b]

[a] *ONERA/DEMR, 2, avenue Édouard Belin, BP4025, 31055 Toulouse cedex, France*
[b] *UPS/AD2M, 118, route de Narbonne, 31062 Toulouse cedex, France*

Available online 2 September 2005

**Abstract**

This article aims to evaluate the abilities of Gaussian beam techniques to compute the interaction between an electromagnetic field and a multilayer dielectric object. First, we propose an approach to expand a field on a set of elementary Gaussian beams from a curved surface. Then, we study two techniques to compute the interaction: a Gaussian beam shooting and bouncing algorithm and another original approach using the Gaussian beam transmission and reflection coefficients. We analyse the advantages (rapidity/accuracy) of these two techniques with respect to a conventional approach to compute the radiation of an antenna protected by a radome. ***To cite this article: A. Chabory et al., C. R. Physique 6 (2005).***


**Résumé**

**Modélisation de la diffraction électromagnétique par des objets diélectriques multicouches par des techniques basées sur les faisceaux gaussiens.** Dans cet article, nous évaluons les possibilités offertes par les techniques basées sur les faisceaux gaussiens pour traiter l'interaction entre un champ électromagnétique et un objet diélectrique multicouche. Nous proposons tout d'abord une nouvelle approche pour décomposer un champ connu sur une surface courbe comme une somme de faisceaux gaussiens élémentaires. Nous étudions ensuite deux techniques pour traiter l'interaction du champ avec l'objet : d'une part un algorithme de lancer de faisceaux gaussiens et d'autre part une approche originale qui s'appuie sur la définition des coefficients de transmission et de réflexion associés au faisceau gaussien. Nous montrons l'intérêt de ces deux techniques (rapidité/précision) par rapport à une approche conventionnelle pour modéliser le rayonnement d'une antenne protégée par un radôme. ***Pour citer cet article : A. Chabory et al., C. R. Physique 6 (2005).***


*Keywords:* Electromagnetic asymptotic methods; Gaussian beams; Radomes; Lenses

*Mots-clés :* Méthodes asymptotiques électromagnétiques ; Faisceaux gaussiens ; Radômes ; Lentilles

## 1. Introduction

The radiation computation of antennas placed behind large dielectric multilayer radomes or lenses requires a compromise between computation time and accuracy. Exact methods, such as the Method of Moments, imply a prohibitive computation

* Corresponding author.
*E-mail address:* sokoloff@cict.fr (J. Sokoloff).

1631-0705/$ – see front matter 
doi:10.1016/j.crhy.2005.06.011

time whereas asymptotic methods, such as Geometrical and Physical Optics, are known to be faster but less accurate. Other asymptotic techniques based on Gaussian beams have been developed and seem to provide both rapidity and accuracy. They have recently been used to study planar aperture radiation [1,2], metallic reflectors [3–5], lenses [6,7] and radomes [8]. Most of these approaches can be applied following two steps.

In the first, the incident field is expanded on a discrete set of elementary beams. One possibility is to choose the vectorial multimodal orthogonal Gauss–Hermite (or Gauss–Laguerre) basis which has been successfully used to express fields scattered by metallic [3] or dielectric [6] objects. However, this expansion strongly depends on the paraxial approximation which requires that the described fields are only weakly diverging along their main propagation direction. Another solution is the Gabor expansion which expresses a signal as a superposition of Gaussian functions placed on a doubly infinite spectral-spatial discrete lattice [9]. Felsen et al. [10] have shown that this expansion allows the representation of planar aperture radiation as a sum of beams shifted both in position and in propagation direction. To avoid the numerical difficulties to determine the expansion coefficients due to the non-orthogonality of the Gaussian functions, two different solutions have been developed. Maciel and Felsen propose the 'Gabor-based narrow waisted Gaussian beam algorithm' [1]. The expansion coefficients are directly obtained by sampling the initial field. Lugara and Letrou replace Gabor basis by the Gabor frame which corresponds to an over-sampling of the elementary beams [2]. Expansion coefficients are then obtained with frame adjoint functions, providing numerical stability. The Gabor expansion, however, presents other limitations: the expansion surface has to be planar and the analytical formulation of the elementary beams does not always correspond to conventional Gaussian beams. Two other expansion techniques have also been developed to express a field as a combination of Gaussian beams shifted both in position and in propagation direction from a planar [4] and from a semi-spherical surface [5]. Although they do not use any base or any frame, but a set of Gaussian beams, they provide good results.

In the second step, the interaction between the elementary beams and the object is investigated. On a dielectric interface, most of the techniques assume that one incident Gaussian beam gives one transmitted and one reflected Gaussian beam [11]. This assumption, combined with an expansion of the incident field, has led to the development of Gaussian beam shooting and bouncing algorithms [7,12].

In this article, we both review expansion and interaction issues. In Section 2, we briefly present Gaussian beams and their analytical formulations. In Section 3, we propose a new pragmatic expansion to express a field known on a regular curved surface as a set of elementary beams shifted both in position and in propagation direction. Then, we analyze in Section 4 two approaches to treat the interaction of an electromagnetic field with a multilayer dielectric object. The first one is a Gaussian beam shooting and bouncing algorithm. The second one is an original approach using the novel Gaussian beam transmission and reflection coefficients. Finally, we give in Section 5 an application of these techniques on a 3-layer dielectric ellipsoidal radome. Concluding remarks follow in Section 6.

## 2. Gaussian beams

Gaussian beams are analytical solutions of the approximated wave equation. They depend on the paraxial approximation which requires that the field is only weakly divergent along its main propagation direction. A maximum divergence angle of $20^\circ$ along this axis is often assumed. The analytical vectorial expression of a Gaussian beam propagating along the $z$-direction is given by:

$$\begin{aligned}\vec{E}(x,y,z) &= a^{(xz)}\left(u(x,y,z)\vec{e}_x - \frac{j}{k}\frac{\partial u(x,y,z)}{\partial x}\vec{e}_z\right) + a^{(yz)}\left(u(x,y,z)\vec{e}_y - \frac{j}{k}\frac{\partial u(x,y,z)}{\partial y}\vec{e}_z\right)\\ \vec{H}(x,y,z) &= \frac{\sqrt{\varepsilon_r}}{Z_0}a^{(xz)}\left(u(x,y,z)\vec{e}_y - \frac{j}{k}\frac{\partial u(x,y,z)}{\partial y}\vec{e}_z\right) - \frac{\sqrt{\varepsilon_r}}{Z_0}a^{(yz)}\left(u(x,y,z)\vec{e}_x - \frac{j}{k}\frac{\partial u(x,y,z)}{\partial x}\vec{e}_z\right)\end{aligned} \tag{1}$$

$\varepsilon_r$ and $k$ are respectively the relative permittivity and the wave number of the medium. $Z_0$ is the free space impedance. $a^{(xz)}$ and $a^{(yz)}$ represent the coefficients associated with the $x$ and $y$ polarization. $u$ stands for the scalar Gaussian beam expression:

$$u(x,y,z) = u_0\frac{\sqrt{\det Q(z)}}{\sqrt{\det Q(0)}}\exp\left[-\frac{jk}{2}\begin{bmatrix}x\\y\end{bmatrix}^t Q(z)\begin{bmatrix}x\\y\end{bmatrix} - jkz\right] \tag{2}$$

$Q(z)$, which represents the beam's complex curvature matrix, is similar to the real curvature matrix in the Geometrical Optics fields [11]. The inverse of this matrix linearly depends on the axial coordinate:

$$Q^{-1}(z) = Q^{-1}(0) + z\begin{bmatrix}1 & 0\\0 & 1\end{bmatrix} \tag{3}$$

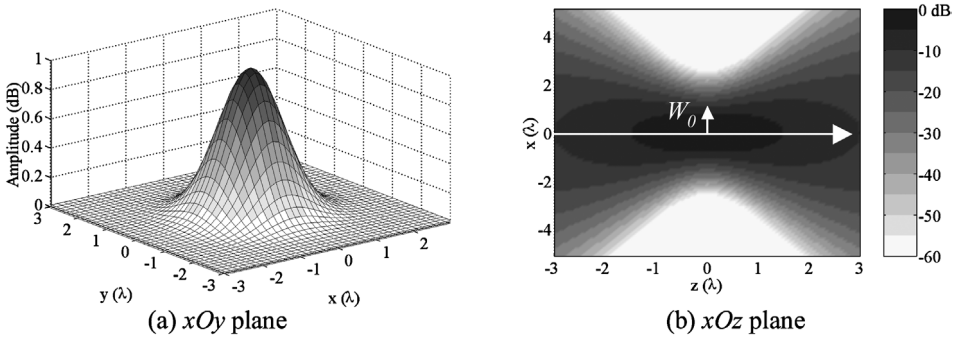


Fig. 1. Circular symmetric Gaussian beam amplitude in transversal and longitudinal planes with $W_0 = \lambda$.

Fig. 1. Amplitude d'un faisceau gaussien à symétrie de révolution dans les plans transversaux et longitudinaux pour $W_0 = \lambda$.

Moreover, $Q(z)$ provides the beam's transversal evolution. It gives both the curvature radii of the wave front on the $z$-axis and the Gaussian transversal variation of the amplitude. For a symmetric circular Gaussian beam, the initial matrix $Q(0)$ only depends on the beam waist size $W_0$ and is given by:

$$Q(0) = \frac{-2j}{kW_0^2}\begin{bmatrix} 1 & 0 \\ 0 & 1 \end{bmatrix} \tag{4}$$

Then, the paraxial approximation usually holds when $kW_0 > 5$, i.e., $W_0 > 0.8\lambda$ where $\lambda$ is the wavelength in the medium. The amplitude of a symmetric circular beam is shown on Fig. 1.

In the far field region, the paraxial approximation produces an important phase error which prevents properly summing beams with different propagation axes. To overcome this limitation, another analytical expression exists which does not depend on the paraxial approximation but on a far field approximation. For a Gaussian beam propagating along the $z$ axis, this far field expression is given by:

$$\vec{E}(r,\theta,\varphi) = E(r,\theta,\varphi)\left[a^{(xz)}(\cos\theta\vec{e}_x - \sin\theta\cos\varphi\vec{e}_z) + a^{(yz)}(\cos\theta\vec{e}_y + \sin\theta\sin\varphi\vec{e}_z)\right] \tag{5}$$

with

$$E(r,\theta,\varphi) = u_0\sqrt{\frac{1}{\det Q(0)}}\exp\left(\frac{jk\sin^2\theta}{2}\begin{bmatrix}\cos\varphi \\ \sin\varphi\end{bmatrix}^t Q^{-1}(0)\begin{bmatrix}\cos\varphi \\ \sin\varphi\end{bmatrix}\right)\frac{\exp(-jkr)}{r} \tag{6}$$

where $r, \theta$ and $\varphi$ are the spherical coordinates. In the next sections, this expression will be used for the far field radiation pattern computation.

Hence, Gaussian beams present local properties with a finite extent on the transverse directions associated with a reduced angular beamwidth radiation. They appear as an intermediate solution between the plane and the spherical waves.

## 3. Expansion of an electromagnetic field in Gaussian beams

In this section, we aim to develop an approach to express an electromagnetic field in terms of a set of conventional Gaussian beams shifted both in position and in propagation direction. Two expansions have previously been proposed. Pathak et al. distribute the elementary beams on a doubly regular spatial/angular planar grid [4]. In order to find the expansion coefficients, a point matching technique is then used by sampling the given field and the beam sum in the far field zone. Lemaître et al. perform the expansion from a semi-spherical surface [5]. The elementary beam centres are placed on a regular mesh of the surface. On each mesh point only one beam is located and oriented along the surface normal vector. The expansion coefficients are then found by means of a point matching technique directly applied on the spherical surface.

Here, we propose an alternative expansion where the initial field $(\vec{E}^i, \vec{H}^i)$ is known on a regular surface whose characteristic dimensions (size, curvature radii) are large with respect to the wavelength (Fig. 2). Each elementary beam has its own reference $(O_n^i, \vec{e}_{xn}^i, \vec{e}_{yn}^i, \vec{e}_{zn}^i)$ where $O_n^i$ stands for the $n$th-beam centre and $(\vec{e}_{xn}^i, \vec{e}_{yn}^i, \vec{e}_{zn}^i)$ respectively represent the $n$th-beam polarization and propagation axes. To take into account the vectorial characteristics of the initial field, each beam may have an $x$-polarized component $\vec{E}_n^{i(xz)}$ and an $y$-polarized component $\vec{E}_n^{i(yz)}$, as shown in (1). Finally, the expansion expression is given by:

$$\vec{E}^i = \sum_{n=1}^{N} a_n^{i(xz)}\vec{E}_n^{i(xz)} + a_n^{i(yz)}\vec{E}_n^{i(yz)} \tag{7}$$

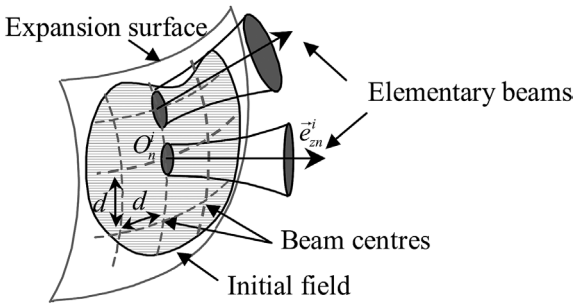


Fig. 2. Gaussian beam expansion principle.

Fig. 2. Principe de la décomposition en faisceaux gaussiens.

Then, the characteristics of each elementary beam have to be determined. The beam centres $O_n^i$ are regularly distributed on the initial surface from a mesh of step $d$. As in [5], only one beam is selected on each beam centre in order to reduce their number. To have a precise description of the local properties of the electromagnetic fields, each elementary beam propagation axis is oriented along the local Poynting vector. Moreover, the elementary beam polarization is chosen so that a given field polarized along a vector $\vec{e}_x^{\,i}$ gives $a_n^{i(yz)}$ expansion coefficients equal to zero. Finally, we obtain:

$$\vec{e}^{\,i}_{zn} = \frac{\Re(\vec{E}^i(O_n^i) \wedge \vec{H}^{i^*}(O_n^i))}{\|\Re(\vec{E}^i(O_n^i) \wedge \vec{H}^{i^*}(O_n^i))\|}, \qquad \vec{e}^{\,i}_{yn} = \frac{\vec{e}^{\,i}_{zn} \wedge \vec{e}^{\,i}_{x}}{\|\vec{e}^{\,i}_{zn} \wedge \vec{e}^{\,i}_{x}\|}, \qquad \vec{e}^{\,i}_{xn} = \vec{e}^{\,i}_{yn} \wedge \vec{e}^{\,i}_{zn} \tag{8}$$

The expansion coefficients are computed by a point matching technique. On the mesh points, we project the equality between the initial electric field and the beam expansion along the two vectors associated to the elementary beam polarization:

$$\begin{cases} \vec{E}^i(O_p^i).\vec{e}^{\,i}_{xp} = \sum_{n=1}^{N} a_n^{i(xz)} \vec{E}_n^{i(xz)}(O_p^i).\vec{e}^{\,i}_{xp} + a_n^{i(yz)} \vec{E}_n^{i(yz)}(O_p^i).\vec{e}^{\,i}_{xp} \\ \vec{E}^i(O_p^i).\vec{e}^{\,i}_{yp} = \sum_{n=1}^{N} a_n^{i(xz)} \vec{E}_n^{i(xz)}(O_p^i).\vec{e}^{\,i}_{yp} + a_n^{i(yz)} \vec{E}_n^{i(yz)}(O_p^i).\vec{e}^{\,i}_{yp} \end{cases} \quad \forall p \in [1, N] \tag{9}$$

Then, the solution of this linear system gives the coefficients.

The characteristics of the elementary beam set only depend on the choice of two related parameters: the waist $W_0$ and the mesh step $d$. Their values affect both the accuracy and the rapidity. Small values of $W_0$ are suitable for a very local description of electromagnetic fields, but it has to comply with the paraxial approximation ($W_0 > 0.8\lambda$). For small $d$ values, the mesh is tight and there is an important number of elementary beams, increasing accuracy but also computation time. However, $d$ and $W_0$ cannot be chosen independently. When we consider the ratio $\kappa = d/W_0$, we can note that large values of $\kappa$ ($d \gg W_0$) lead to a sparse distribution of beams, unable to describe properly the fields between the mesh points. On the other hand, small values of $\kappa$ ($d \ll W_0$) correspond to overlaying strongly coupled beams, making the point matching technique inefficient. A comprehensive parametric study using various initial fields, incidences and surfaces has confirmed these expected results [13]. It has been shown that a good compromise between accuracy and computation time was achieved with $\kappa \cong 0.9$, and $d$ varying between $\lambda$ and $2\lambda$.

The test referred to in Section 5.1 illustrates the good performances of this expansion. However, this technique is limited since each elementary beam must be local on a limited area of the expansion surface. This implies that the initial field incidence and the surface curvature must remain moderate.

## 4. Interaction between an electromagnetic field and a multilayer dielectric object

### *4.1. Shooting and bouncing Gaussian beam algorithm*

A first approach to treat multilayer dielectric objects with Gaussian beam techniques is a shooting and bouncing beam algorithm. It combines the incident field expansion presented above and the assumption that one incident Gaussian beam on a dielectric interface generates only one transmitted and one reflected Gaussian beam.

First, we present the well-known approach to treat the transformation of each incident Gaussian beam on an interface separating two dielectric media with relative permittivity $\varepsilon_{r1}$ and $\varepsilon_{r2}$ [11]. On Fig. 3(a), we define the local references $li$, $lr$ and $lt$ respectively associated with the incident, reflected and transmitted beams and the local reference $\Sigma$ associated with the interface. They are defined with respect to the incidence plane and they are centred in $I$, the intersection point between the incident propagation axis and the interface.

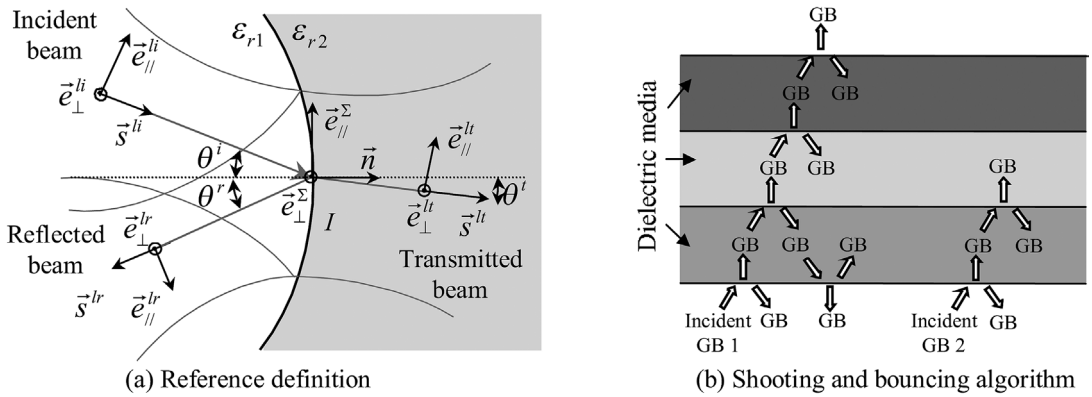


Fig. 3. Gaussian beam shooting and bouncing approach.

Fig. 3. Approche du lancer de faisceaux gaussiens.

The incident Gaussian beam coefficients and initial curvature matrix are expressed in the local incidence reference. They are respectively denoted $a^{i(\parallel)}$, $a^{i(\perp)}$ and $Q^{li}(O)$. Then, the transmitted and reflected beams characteristics (references, curvature matrix amplitudes) must be determined. Their propagation axis and their curvature matrix can be evaluated by the phase matching principle which imposes a second order equality between the exponential terms of all the beams. It implies that the propagation axes satisfy the Snell–Descartes laws ($\theta^r = \theta^i$ and $\sqrt{\varepsilon_{r1}}\sin\theta^i = \sqrt{\varepsilon_{r2}}\sin\theta^t$) and the complex curvature matrices are given by:

$$
\begin{aligned}
Q^{lr}(0) &= \begin{pmatrix} Q^{li}_{11}(0) - 2\dfrac{Q^{\Sigma}_{11}}{\cos\theta^i} & 2Q^{\Sigma}_{12} - Q^{li}_{12}(0) \\ 2Q^{\Sigma}_{12} - Q^{li}_{12}(0) & Q^{li}_{22}(0) - 2\cos\theta^i\, Q^{\Sigma}_{22} \end{pmatrix} \\
Q^{lt}(0) &= \sqrt{\frac{\varepsilon_{r1}}{\varepsilon_{r2}}} \begin{pmatrix} \dfrac{\cos^2\theta^i}{\cos^2\theta^t} Q^{li}_{11}(0) & \dfrac{\cos\theta^i}{\cos\theta^t} Q^{li}_{12}(0) \\ \dfrac{\cos\theta^i}{\cos\theta^t} Q^{li}_{12}(0) & Q^{li}_{22}(0) \end{pmatrix} + \frac{\sqrt{\varepsilon_{r2}}\cos\theta^t - \sqrt{\varepsilon_{r1}}\cos\theta^i}{\sqrt{\varepsilon_{r2}}} \begin{pmatrix} \dfrac{Q^{\Sigma}_{11}}{\cos^2\theta^t} & \dfrac{Q^{\Sigma}_{12}}{\cos\theta^t} \\ \dfrac{Q^{\Sigma}_{12}}{\cos\theta^t} & Q^{\Sigma}_{22} \end{pmatrix}
\end{aligned}
\tag{10}
$$

$Q^{\Sigma}$ stands for the surface curvature matrix in $I$. Moreover, to estimate the reflected and transmitted beam coefficients, we use the Fresnel coefficients in $I$ leading to:

$$
\begin{aligned}
a^{r(\parallel)} &= \frac{\sqrt{\varepsilon_{r2}}\cos\theta^i - \sqrt{\varepsilon_{r1}}\cos\theta^t}{\sqrt{\varepsilon_{r1}}\cos\theta^t + \sqrt{\varepsilon_{r2}}\cos\theta^i} a^{i(\parallel)}, \qquad a^{t(\parallel)} = \frac{2\sqrt{\varepsilon_{r1}}\cos\theta^i}{\sqrt{\varepsilon_{r1}}\cos\theta^t + \sqrt{\varepsilon_{r2}}\cos\theta^i} a^{i(\parallel)} \\
a^{r(\perp)} &= \frac{\sqrt{\varepsilon_{r1}}\cos\theta^i - \sqrt{\varepsilon_{r2}}\cos\theta^t}{\sqrt{\varepsilon_{r1}}\cos\theta^i + \sqrt{\varepsilon_{2}}\cos\theta^t} a^{i(\perp)}, \qquad a^{t(\perp)} = \frac{2\sqrt{\varepsilon_{r1}}\cos\theta^i}{\sqrt{\varepsilon_{r1}}\cos\theta^i + \sqrt{\varepsilon_{r2}}\cos\theta^t} a^{i(\perp)}
\end{aligned}
\tag{11}
$$

In the shooting and bouncing algorithm, each elementary Gaussian beam, denoted GB on Fig. 3(b), is tracked through the dielectric media. When it reaches an interface, it generates two new beams (transmitted and reflected) which are then tracked in turn. All different beams are treated the same way and the algorithm is stopped according to a beam power lower limit. Finally, the fields in the entire space can be computed as a sum of Gaussian beams.

The accuracy of this algorithm is limited by the assumption that one Gaussian beam gives only Gaussian beams through a dielectric interface. Its computation time depends on the number of beams generated by the algorithm and exponentially increases with the number of layers.

### *4.2. Approach based on Gaussian beam reflection and transmission coefficients*

We propose an original approach based on the definition of novel Gaussian beam reflection and transmission coefficients. In this subsection, these coefficients are first defined. Then, a fast iterative process is proposed to compute multilayer dielectric objects.

The Gaussian beam reflection and transmission coefficients are obtained from a conventional technique using the plane wave spectrum representation [16]. We consider a dielectric interface between two media with relative permittivity $\varepsilon_{r1}$ and $\varepsilon_{r2}$ illuminated by an incident field associated to an incident reference $(O^i, \vec{e}_x^i, \vec{e}_y^i, \vec{e}_z^i)$. On the interface point $I$, the incident field can be written as:

$$\vec{E}^i(I) = \frac{1}{4\pi^2} \int_{-\infty}^{+\infty}\int_{-\infty}^{+\infty} \hat{\vec{E}}^i(k_x^i, k_y^i) \exp\bigl(-j\vec{k}^i \cdot \overrightarrow{O^i I}\bigr)\, \mathrm{d}k_x^i\, \mathrm{d}k_y^i \tag{12}$$

where $\vec{k}^i = (k_x^i, k_y^i, k_z^i)$ are the plane wave vectors expressed in the incident reference. If $k_1$ is the wave number in the first medium, the $k_z^i$ component is obtained from $k_1^2 = {k_x^i}^2 + {k_y^i}^2 + {k_z^i}^2$. $\hat{\vec{E}}^i$ represents the plane wave spectrum and corresponds to the spatial Fourier transform of the field at $z^i = 0$:

$$\hat{\vec{E}}\bigl(k_x^i, k_y^i\bigr) = \int_{-\infty}^{+\infty}\int_{-\infty}^{+\infty} \vec{E}\bigl(x^i, y^i, 0\bigr) \exp\bigl(jk_x^i x^i + jk_y^i y^i\bigr)\, \mathrm{d}x^i\, \mathrm{d}y^i \tag{13}$$

Using the local tangent plane approximation, the reflected and transmitted field expressions on $I$ can be written as:

$$\begin{aligned}
\vec{E}^r(I) &= \frac{1}{4\pi^2} \int_{-\infty}^{+\infty}\int_{-\infty}^{+\infty} \overline{\overline{R}}\bigl(\vec{k}^i, \vec{n}(I)\bigr) \hat{\vec{E}}^i\bigl(k_x^i, k_y^i\bigr) \exp\bigl(-j\vec{k}^i \cdot \overrightarrow{O^i I}\bigr)\, \mathrm{d}k_x^i\, \mathrm{d}k_y^i \\
\vec{E}^t(I) &= \frac{1}{4\pi^2} \int_{-\infty}^{+\infty} \int_{-\infty}^{+\infty} \overline{\overline{T}}\bigl(\vec{k}^i, \vec{n}(I)\bigr) \hat{\vec{E}}^i\bigl(k_x^i, k_y^i\bigr) \exp\bigl(-j\vec{k}^i \cdot \overrightarrow{O^i I}\bigr)\, \mathrm{d}k_x^i\, \mathrm{d}k_y^i
\end{aligned} \tag{14}$$

where $\overline{\overline{R}}$ and $\overline{\overline{T}}$ are the dyadic Fresnel coefficients depending both on the plane wave propagation axis and on the local tangent plane orientation. In the conventional approach, to obtain the reflected and transmitted fields on the interface, these two integrals must be numerically computed, which can be time consuming.

The Gaussian beam coefficients are developed to suppress these numerical integrations. Considering now an incident Gaussian beam, its analytical expression (1) combined with (13) provides a Gaussian analytical expression for the spectrum:

$$\hat{\vec{E}}(k_x^i, k_y^i) = \frac{2\pi j}{k_1\sqrt{\det Q^i(0)}} \exp\left(\frac{j}{2k} \begin{bmatrix} k_x^i \\ k_y^i \end{bmatrix}^t Q^{-1}(0) \begin{bmatrix} k_x^i \\ k_y^i \end{bmatrix}\right)\left(a^{i(xz)}\vec{e}_x^i + a^{i(yz)}\vec{e}_y^i - \frac{a^{i(xz)}k_x^i + a^{i(yz)}k_y^i}{k_z^i}\vec{e}_z^i\right) \tag{15}$$

Assuming the paraxial approximation and slowly varying $\overline{\overline{R}}$ and $\overline{\overline{T}}$ coefficients, the asymptotic evaluation of the integrals (14) with the steepest descent path method [14] gives analytical expressions for the reflected and transmitted fields on the interface:

$$\vec{E}^r(I) = \overline{\overline{R}}\bigl(\vec{k}^{is}, \vec{n}(I)\bigr)\vec{E}^i(I) = \overline{\overline{R}}_{\mathrm{GB}}(I)\vec{E}^i(I), \qquad \vec{E}^t(I) = \overline{\overline{T}}\bigl(\vec{k}^{is}, \vec{n}(I)\bigr)\vec{E}^i(I) = \overline{\overline{T}}_{\mathrm{GB}}(I)\vec{E}^i(I) \tag{16}$$

The $x$ and $y$ components of $\vec{k}^{is}$ correspond to the saddle point of the steepest descend path method. They are given by:

$$\begin{bmatrix} k_x^{is} \\ k_y^{is} \end{bmatrix} = k_1 Q(z) \begin{bmatrix} x^i \\ y^i \end{bmatrix}, \qquad k_z^{is} = k_1 - \frac{k_x^{is^2} + k_y^{is^2}}{2k_1} \tag{17}$$

$\overline{\overline{R}}_{\mathrm{GB}}$ and $\overline{\overline{T}}_{\mathrm{GB}}$ define the novel dyadic coefficients associated with the Gaussian beam. They provide analytical expressions of the transmitted and reflected fields on a dielectric interface illuminated by a Gaussian beam. These expressions can be combined with the previous expansion for dielectric multilayer object computation.

An iterative solution technique has been developed [15], as illustrated on Fig. 4. As usual, the incident field is expanded in Gaussian beams. Then, on the first interface, the transmitted and reflected fields are computed with (16). The transmitted field is expanded whereas the reflected field is stored at level {1}. On the following interfaces, the same process is applied. On the last one, the procedure is reversed, the transmitted field is stored at $\{M\}$ whereas the reflected field is expanded. The process then crosses the object in the other direction. On the last but one interface, the transmitted field is added to $\{M-1\}$ and expanded. After that, the reflected field is stored at $\{M-1\}$. This process is repeated until field power reaches a given limit. Finally, the fields on the first and last interfaces respectively correspond to the sum of level {1} and to the sum of level $\{M\}$. They are expanded in Gaussian beams in order to obtain the fields reflected and transmitted by the object. This process will remain efficient for objects with many layers because its computation time linearly depends on the number of layers.

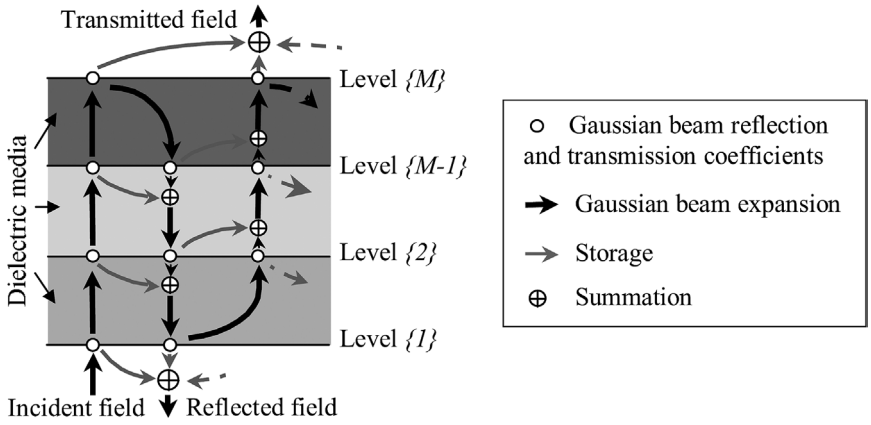


Fig. 4. Process based on Gaussian beam reflection and transmission coefficients.

Fig. 4. Processus basé sur les coefficients de réflexion et de transmission d'un faisceau gaussien.

## 5. Application

### 5.1. Example of a field expansion

To test the expansion efficiency on a curved surface, we expand an initial field on a semi-spherical surface. This field is radiated by a planar aperture placed in $z^i = 0$ (Fig. 5(a)). The electric field distribution in the aperture is linearly polarized along the $x$-axis and given by:

$$E_x^i = \begin{cases} \cos\dfrac{\pi\rho^i}{L} & \text{if } |\rho^i| < L/2 \text{ with } \rho^i = \sqrt{x^{i2} + y^{i2}} \\ 0 & \text{elsewhere} \end{cases} \tag{18}$$

The aperture width is $L = 8\lambda$ and the frequency is 10 GHz. The expansion is performed on a semi-spherical surface centred on the aperture with a radius of $12\lambda$. The expansion parameters are $d = \lambda$ and $\kappa = 0.9$. In a preliminary stage, the initial field is obtained on this surface thanks to the Kottler radiation integrals. Then, the expansion coefficients are computed by solving the linear system (9). This expansion requires 850 beams and needs 17 s on a PC 3 GHz CPU.

On Fig. 5(b), we show the field in the $E$-plane at $z^i = 10\lambda$ obtained from the Gaussian beam sum and from the Kottler radiation integrals. We observe that the Gaussian beam sum takes correctly into account the field propagation in the near field region. On Fig. 5(c), we represent the far field radiation pattern in the $E$-plane. Here, we recall that Gaussian beams must be computed with their far field expression (5). We note a very good agreement between the two results. Moreover, we have verified that the vectorial difference is below $-60$ dB.

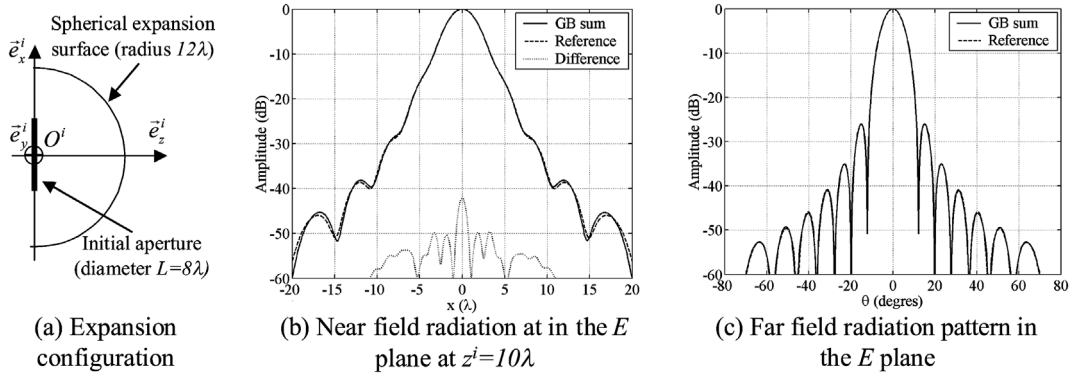


(a) Expansion configuration

(b) Near field radiation at in the $E$ plane at $z^i=10\lambda$

(c) Far field radiation pattern in the $E$ plane

Fig. 5. Comparisons between the Gaussian beam expansion and the Kottler radiation integrals.

Fig. 5. Comparaisons entre la décomposition en faisceaux gaussiens et les intégrales de rayonnement de Kottler.

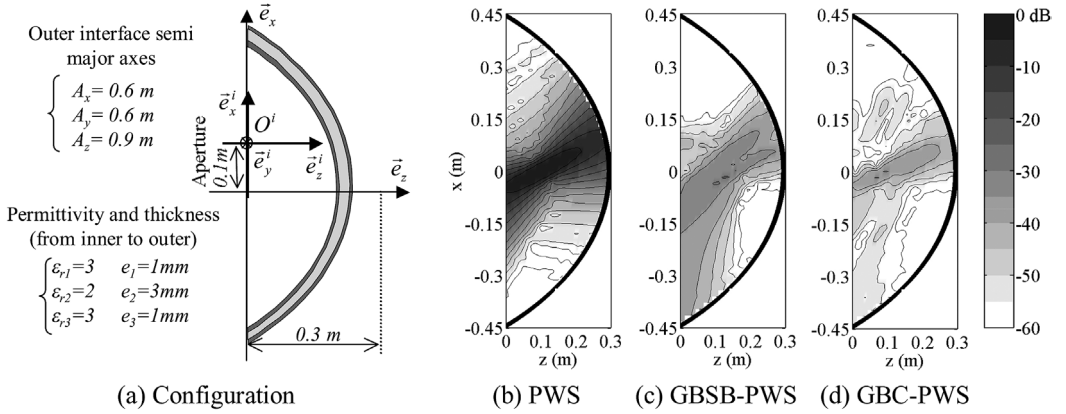


Fig. 6. Radome configuration and reflected field cartographies in the $E$-plane.

Fig. 6. Configuration du radôme et cartographies du champ réfléchi dans le plan $E$.

### *5.2. Radome computation*

As an application of both approaches presented in Section 4, we place the aperture of the example above under an ellipsoidal 3-layer radome. The configuration is detailed on Fig. 6(a). First, we compute the reflected field in the $E$-plane with a conventional plane wave spectrum approach denoted PWS [16]. Fig. 6(b) represents this field. On Fig. 6(c), the vectorial difference between the conventional approach and the Gaussian beam shooting and bouncing algorithm (denoted GBSB) is shown. We observe that the difference remains below $-30$ dB everywhere. Fig. 6(d) represents the difference between the conventional approach and the process based on Gaussian beam coefficients (denoted GBC). The result is slightly better since the difference here is below $-35$ dB. Concerning the rapidity, the total computation times are respectively 46 min 35 s for PWS, 1 min 18 s for GBSB and 1 min 39 s for GBC. We note that the two Gaussian beam based techniques approximately give the same time and are faster than the PWS approach. Thanks to the linear evolution of its computation time, GBC will become faster than GBSB for a radome with multiple layers.

## 6. Conclusion

First, the expansion of a field in a set of elementary Gaussian beams on a curved surface has been developed and analysed. Then, two Gaussian beam approaches to treat multilayer dielectric objects have been presented and tested. The first one is a shooting and bouncing algorithm using the well-known assumption that one incident Gaussian beam only gives Gaussian beams through a dielectric interface. The other one is based on the novel Gaussian beam transmission and reflection coefficients. They provide the transmitted and reflected fields on a dielectric interface illuminated by a Gaussian beam. Concerning the rapidity, both have led to very good performances compared to a conventional radome approach. Furthermore, GBC shows an interesting linear evolution of computation time with the number of layers thanks to a judicious iterative process. Concerning the accuracy, the comparisons with PWS have been very satisfactory. For objects with thicker layers or with non-constant thicknesses, we expect that Gaussian beam techniques may provide better accuracy than PWS. Indeed, to take into account multiple reflections, they use iterative processes contrary to PWS which uses global multilayer Fresnel coefficients. To demonstrate this ability, we intend to make comparisons with other reference results (measurements, numerical methods, ...).

Finally, this article has shown the abilities of two Gaussian beam techniques to compute the interaction between an electromagnetic field and a large dielectric multilayer object. Some improvements are now being investigated to treat more general shapes and more complex structures. To compute sharp nose aircraft radomes, we are looking for new expansions overcoming the limitations due to high incidence angles and high curvatures. We also want to take into account the effects of metallic parts on the radome (metallic tip, lightning protector strips). It leads us to the general issue of searching new analytical formulations in order to treat the diffraction of a Gaussian beam by a metallic surface with sharp edges.

## References

[1] J.J. Maciel, L.B. Felsen, Discretized Gabor-based beam algorithm for time harmonic radiation from two dimensional truncated planar aperture distributions I—Formulation and solution, II—Asymptotics and numerical tests, IEEE Trans. Antennas Propag. 50 (2002).

[2] D. Lugara, C. Letrou, Alternative to Gabor's representation of plane aperture radiation, Electron. Lett. 34 (1998).
[3] J. Sokoloff, S. Bolioli, P.F. Combes, Gaussian beam expansion for radiation analysis of metallic reflectors illuminated under oblique incidence, IEEE Trans. Mag. 38 (2002).
[4] H.T. Chou, P.H. Pathak, R.J. Burkholder, Novel Gaussian beam method for the rapid analysis of large reflector antennas, IEEE Trans. Antennas Propag. 49 (2001).
[5] P. Schott, F. Lemaître, O. Pascal, Use of Gaussian beams to compute antenna pattern, Ann. Télécom. 57 (2002).
[6] O. Pascal, F. Lemaitre, G. Soum, Paraxial approximation effect on a dielectric interface analysis, Ann. Télécom. 51 (1996).
[7] D. Lugara, A. Boag, C. Letrou, Gaussian beam tracking through a curved interface: comparison with a method of moments, IEE Proc. Microwave Antennas Propag. 150 (1996).
[8] J.J. Maciel, L.B. Felsen, Gabor-based narrow waisted Gaussian beam algorithm for transmission of aperture-excited 3D vector fields through arbitrarily shaped 3D dielectric layers, Radio-Science 38 (2003).
[9] D. Gabor, Theory of communication, J. Inst. Elec. Ing. 93 (1946).
[10] P.D. Eiziger, Y. Haramaty, L.B. Felsen, Complex rays for radiation from discretized aperture distribution, IEEE Trans. Antennas Propag. 35 (1987).
[11] G.A. Dechamps, Ray techniques in electromagnetics, Proc. IEEE 60 (1972).
[12] R.J. Burkholder, P.H. Pathak, Analysis of EM penetration into and scattering by electrically large open waveguide cavities using Gaussian beam shooting, Proc. IEEE 79 (1991).
[13] A. Chabory, Modélisation électromagnétique des radômes par des techniques basées sur les faisceaux gaussiens, Thèse de l'Université Toulouse III, 2004.
[14] L.B. Felsen, N. Marcuvitz, Radiation and Scattering of Waves, Prentice-Hall, New York, 1973.
[15] A. Chabory, J. Sokoloff, S. Bolioli, P.F. Combes, Fast Multilayer radome computation with Gaussian beams, in: URSI 2004 Proceedings, 2004.
[16] D.C. Wu, R.C. Rudduck, Plane wave spectrum surface integration technique for radome analysis, IEEE Trans. Antennas Propag. 22 (1974).